**CONFERENCE PRE-PRINT**

# UK STEP TOWARDS A FUSION POWER PLANT PLASMA

[1]H. MEYER, [2]F.J. CASSON, [2]N. CONWAY, [2]S. FREETHY, [2]T. C. HENDER, [2]M. HENDERSON, [2]S. HENDERSON, [2]K. KIROV, [2]M. LENNHOLM, [2]K.G. MCCLEMENTS, [2]J. MORRIS, [2]C.M. ROACH, [2]S. SAARELMA, [2]D. VALCARCEL AND THE STEP PLASMA TEAM

[1]UK Industrial Fusion Solution Ltd. (UKAEA Group), Abingdon, UK
[2]United Kingdom Atomic Energy Authority (UKAEA Group), Abingdon, UK
Email: hendrik.meyer@ukifs.uk

**Abstract**

STEP is a UK programme to build a prototype fusion power plant targeting 2040 demonstrating fuel self-sufficiency and net electric power output of the order of 100 MW [1]. The plasma scenario is central to the STEP mission. Progress has been made in the understanding of the underlying physics and integration of the scenario components with increasing modelling capability. A first existence demonstration of the flat-top operating point is given using a predictive flux-driven quasilinear model describing the transport in STEP. A recent size change for technical reasons necessitated a redevelopment of the scenario, showing some clear disadvantages of a larger device. An overview of the scenario work is presented.

## 1. INTRODUCTION

Central to the design of STEP is a highly elongated, fully non-inductive (NI) plasma solution [2] as well as its control [3]. The current required in addition to the intrinsic bootstrap current ($f_{\mathrm{BS}} = I_{\mathrm{BS}}/I_{\mathrm{p}} \sim 0.8 - 0.9$) is provided solely by microwave-based heating and current drive (HCD). Options have been explored for (1) electromagnetic electron cyclotron wave current drive (ECCD) alone, and (2) a mix of on-axis ECCD and off-axis electrostatic electron Bernstein waves (EBCD) [4]. The normalised current drive efficiency for EBCD is predicted to be three times higher than ECCD, opening up the possibility to access a $Q_{\mathrm{fus}} = P_{\mathrm{fus}}/P_{\mathrm{aux}} \sim 30$ flat-top operation point (FTOP) compared to the ECCD only $Q_{\mathrm{fus}} \sim 11$ FTOP required for a net electricity output $P_{\mathrm{net}}^{el} > 100$ MW [2,5]. The published design point (SPP-1) with $R_{\mathrm{geo},1} = 3.6$ m, $A = 1.8$, $B_t(R_{\mathrm{geo}}) = 3.2$ T, which is predicted to generate $P_{\mathrm{fus}} \sim 1.5 - 1.8$ GW [2], has proven to be technically challenging for the shielding of the toroidal field coils due to the very limited inner build radius of $R_{\mathrm{ib},1} = 1.5$ m. This has led to a design pivot to explore a larger design point (SPP-2) with $R_{\mathrm{geo},2} = 4.3$ m with the same aspect ratio and fusion power, while continuing to pursue ways to reduce the size and the challenges to the plasma solution. In all cases, STEP plasma parameters are far from today's experimentally accessible regimes. Substantial work on both of these fully non-inductive design points has: extended the theoretical basis, reduced the uncertainty of the scenario and its control [3] and developed operating scenarios. This paper gives an overview of the impact of the size change, and the more advanced understanding of the physics base for the STEP plasma scenario and its control.

## 2. THE FLAT TOP OPERATING POINTS (FTOP)

In the absence of validated and sufficiently fast predictive transport models, the initial integrated scenario modelling is used as an assumption integration tool, with a Bohm-gyroBohm (BgB) transport model scaled to give a requested $\beta_N$ within MHD limits, which is then assessed against confinement scalings and higher fidelity transport modelling [2,5]. The possible scenario space is constrained by 7 conditions [5] including the divertor heat load $\frac{P_{\mathrm{sep}}}{R_{\mathrm{geo}}} < 40\,\frac{\mathrm{MW}}{\mathrm{m}}$, $Q_{\mathrm{fus}} > 10$ and $q_{min} > 2.3$, ($P_{\mathrm{sep}}$: power flowing over the separatrix, $q_{\mathrm{min}}$: Minium of the safty factor profile) and optimised with the aim of minimising the confinement assumption with respect to empirical scaling laws (e.g $H_{98(y,2)}$). In principle, the governing quantity to design the fusion power of the FTOP to is the net electric output [6]

$$P_{\mathrm{net}}^{\mathrm{el}} \approx \left[G + \frac{1}{Q_{\mathrm{fus}}}\right] \times P_{\mathrm{fus}} \times \eta_{\mathrm{th}} - L_1 \times \left[\frac{1}{Q_{\mathrm{fus}}\eta_{\mathrm{HCD}}} + L_2\right] \times P_{\mathrm{fus}} - P_{\mathrm{waste}},$$

with $\eta_{\mathrm{th}} \sim 0.35 - 0.4$ the effective thermal efficiency, $\eta_{\mathrm{HCD}} \sim 0.4$ the wallplug efficiency of the HCD system $G$ and $L_{1,2}$ design specific constants accounting for gains and losses to the power production largely proportional to $P_{\mathrm{fus}}$ and $P_{\mathrm{waste}} \sim 100$ MW the loss power that is independent of $P_{\mathrm{fus}}$ such as the magnets loads, building services and computing. This simplified equation is used as a guide in the scenario development to optimise fusion power, heating power and fusion gain.

In [2,5] four FTOPs were developed for SPP-1. Two ECCD only points (EC-HD) with $f_{\mathrm{GW}} = \bar{n}/n_{\mathrm{GW}} \sim 1$ ($n_{\mathrm{GW}} = \frac{I_p}{\pi a^2}$; Greenwald density) and EC-LD with $f_{\mathrm{GW}} \sim 0.6$ optimised to different confinement scaling laws and two dominant EBCD points with a small fraction of on-axis ECCD to avoid a current hole. The higher normalised current drive efficiency of the EBCD can either be used to reduce the assumption on confinement (EB-CC) or to reduce the auxiliary power requirement to drive the current at a similar confinement assumption as for the ECCD

operating point leading to a high fusion gain $Q_{\mathrm{fus},1}^{\mathrm{EB\text{-}HQ}}$~30 (EB-HQ) and high $P_{\mathrm{net},1}^{\mathrm{el,EB\text{-}HQ}}$~0.3 GW. All the scenarios assume Xe as a core radiator, Ar as an edge and divertor radiator as well as the self-consistently produced He from the fusion reaction. The first wall material W is not yet incorporated in the modelling assuming that a small W concentration could be offset by the controllable Xe concentration, though the difference in radiation profiles needs to be studied. For SPP-1 the transport assumptions in the BgB model were chosen to give high electron transport and near neoclassical ion transport as commonly observed in present day STs as well as expected from transport due to micro tearing mode (MTM) turbulence believed at that time to be the dominant heat and particle transport channel.

Improved understanding of the transport in STEP (see section 3) now shows that hybrid kinetic ballooning mode (hKBM) turbulence is the dominant mechanism. For the larger SPP-2 concept the BgB transport assumptions were adjusted to represent hKBM transport. This led to a reduced density peaking as a weaker particle pinch is expected as well as higher fraction of ion to electron heat transport. Keeping 1.5 GW$\leq P_{\mathrm{fus}} \leq$ 1.8 GW and $P_{\mathrm{aux}} \approx$ 150 MW interestingly leads to $I_p \approx$ 21 MA like for SPP-1. The larger minor radius leads to a lower $n_{\mathrm{GW}}$ at a similar current and at $f_{\mathrm{GW}} \approx 1$ a similar fusion power is achieved at overall lower density and slightly lower $\beta_N$ corresponding to the large volume. The resulting lower bootstrap current is compensated by a higher ECCD efficiency. A lower pedestal pressure is predicted as the poloidal field at the edge is reduced and the FTOP assumption integration results in a higher temperature peaking in SPP-2 than in SPP-1.

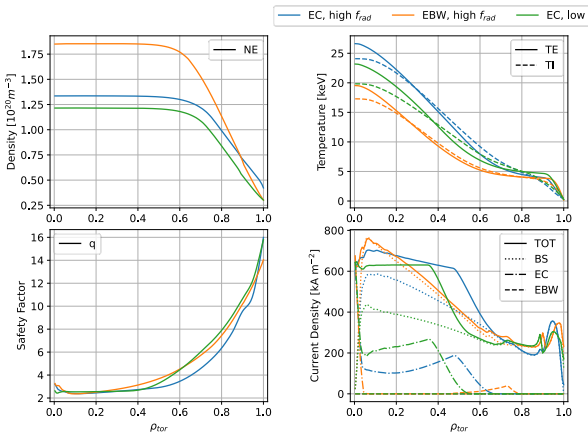


| | EC, high $f_{rad}$ | EBW, high $f_{rad}$ | EC, low $f_{rad}$ |
|---|---|---|---|
| $I_P$ [MA] | 21.50 | 20.13 | 19.12 |
| $B_T$ [T] | 3.0 | 3.0 | 3.0 |
| $P_{FUS}$ [GW] | 1.76 | 1.76 | 1.25 |
| $P_{net}$ [MW] | 177.65 | 415.87 | 140.37 |
| $f_{BS}$ [%] | 85.1 | 96.1 | 83.7 |
| $P_{ECI}$ [MW] | 174.0 | 0.7 | 104.4 |
| $P_{EBW}$ [MW] | 0.0 | 59.8 | 0.0 |
| $\eta_{ECCD}$ [kA/MW] | 18.4 | 31.1 | 29.9 |
| $\eta_{EBWCD}$ [kA/MW] | 0.0 | 12.9 | 0.0 |
| $\eta_{CD}$ [kA/MW] | 18.4 | 13.3 | 29.9 |
| $Q$ | 10.1 | 29.1 | 12.0 |
| $<n_e>$ [$10^{20}$m$^{-3}$] | 1.15 | 1.50 | 1.02 |
| $f_{GW}$ [%] | 100.0 | 140.0 | 100.0 |
| $<T_e>$ [keV] | 10.44 | 7.38 | 9.31 |
| $<T_i>$ [keV] | 10.74 | 7.40 | 9.24 |
| $Z_{eff}$ | 3.26 | 1.38 | 1.49 |
| $f_{rad}$ [%] | 71.95 | 70.08 | 41.26 |
| $P_{sep}/R$ [MW/m] | 31.48 | 26.62 | 47.03 |
| $q_{min}$ | 2.38 | 2.36 | 2.43 |
| $q_0$ | 3.21 | 3.26 | 2.62 |
| $\beta_N$ [%] | 4.20 | 4.10 | 3.78 |
| $\beta_e$ | 0.06 | 0.06 | 0.05 |
| $\beta_{tor}$ | 0.13 | 0.11 | 0.10 |
| Li(3) | 0.33 | 0.28 | 0.30 |
| H98 Avg | 1.39 | 1.36 | 1.31 |
| $\rho_0/<\rho>$ | 2.77 | 2.96 | 2.72 |

*Figure 1 Typical profiles and parameters of an (blue) EC-HD, (orange) EB-HQ and (green) an alternative lower radiation fraction $f_{rad}$ = 40% (EC-LR) FTOP for SPP-2. Note, for the EB-HQ and EC-LR Ar has not yet been included in the self-consistently modelled impurity mix leading to a much lower effective charge, $Z_{eff}$~1.4 compared to 3.3.*

Figure 1 shows typical profiles and parameters for selected FTOPs for SPP-2. The scenarios correspond to (blue, EC-HD) ECCD only, $f_{\mathrm{rad}}$~0.7 and $f_{\mathrm{GW}} = 1$, (orange, EB-HQ) dominant EBCD, $f_{\mathrm{rad}}$~0.7 and $f_{\mathrm{GW}} = 1.4$ and (green, EC-LR) an ECCD only low radiation $f_{\mathrm{rad}}$~0.4 at $f_{\mathrm{GW}} = 1$ variant that has some attractive features due to reduced $P_{\mathrm{fus}}$~ 1.3 GW and slightly lower $I_p$ but requires a better performing divertor with a ~30% higher $P_{\mathrm{sep}}/R_{\mathrm{geo}}$ ~47 MW/m ($P_{\mathrm{sep}}$: power flowing over the separatrix) as more power needs to be exhausted in the divertor. It remains to be seen if this requirement is compatible with a tolerable edge Ar concentration, $c_{\mathrm{Ar}}^{\mathrm{sep}}$ or divertor pressure, $p_{\mathrm{div}}$ (see section 5). For the EB-HQ, EC-LR FTOPs Ar has not yet been self-consistently included in the impurity mix modelling leading to a lower effective charge, $Z_{\mathrm{eff}}$~1.4.

The lower density allows for a slight reduction in $B_t(R_{\mathrm{geo}}) = 3.0$ T, whilst keeping access to 2$^{\mathrm{nd}}$ harmonic O-mode ECCD in the centre. This reduction was supported by a scan in $B_t$ and $f_{\mathrm{GW}}$ to find the optimal solution for current drive. With respect to the absolute current drive efficiency, $\eta_{\mathrm{CD}}$, the profile changes mentioned above are advantageous for the ECCD only scenarios and detrimental for the dominant EBCD scenarios. To recover EBCD performance, the high field side pellet launch was optimised for deeper penetration and FTOPs with $f_{\mathrm{GW}} > 1$ are explored. With these optimisations the EB-HQ scenarios could be recovered and FTOPs have been generated with $Q_{\mathrm{fus}}$~30 at $f_{\mathrm{GW}} = 1.4$ (see Figure 1) and $f_{\mathrm{GW}} = 1.0$. Operating stationarily above the empirical Greenwald density limit has been demonstrated on medium sized tokamaks [7,8] with deep pellet fuelling and transiently on MAST [9] with pellet and gas fuelling. In SPP-1 the ion heating by the $\alpha$-particles led to $T_i > T_e$ in the core. With the new transport assumptions with stronger ion heat transport now $T_i < T_e$ in SPP-2.

The pedestal performance plays a crucial role for the scenario performance. Under the assumption that a pedestal pressure close to the peeling-ballooning stability boundary relevant for type-I ELMs can be achieved the pedestal pressure can be predicted to about 20% accuracy. For the scenario performance, however, both the density and temperature pedestal are individually important and hence the actual transport inside the pedestal is of relevance affecting impurity transport through the pedestal, current drive efficiency, $\eta_{\mathrm{CD}}$, edge bootstrap current and therefore the internal inductance $l_i$. In addition, the edge pedestal gives the boundary condition for the core heat and particle transport. The $\beta$ stabilisation of the peeling ballooning mode may lead to an unphysical feedback loop.

## 3. CORE TRANSPORT

A key caveat of the FTOP development is the lack of a predictive core transport model fully incorporated into JETTO. Nonlinear gyrokinetic (NL-GK) simulations using the derived profiles show that the turbulent transport in STEP is dominated by hybrid kinetic ballooning modes (hKBMs) with subdominant micro-tearing modes (MTM) [10]. The hKBM turbulence can cause unsustainable transport fluxes. Local NL-GK simulations show that the heat flux due to hKBM turbulence is strongly reduced by flow shear and shows a non-monotonic behaviour with electron $\beta_e$ if $\beta_e'$ is varied self-consistently. In the latter simulations the heat flux first increases with increasing $\beta_e$ below a certain critical $(\beta_e, \beta_e')_{\text{crit}}$ before stabilisation by $\beta_e'$ ($\alpha$-stabilisation) leads to a decreasing heat flux with increasing $\beta_e$. Clearly reaching the $(\beta_e, \beta_e') > (\beta_e, \beta_e')_{\text{crit}}$ turbulence regime could lead to a runaway situation if there is no other transport mechanism that limits the increase in $(\beta_e, \beta_e')$ before potentially disruptive global MHD limits are encountered. The subdominant MTM transport could become crucial. The initial analysis of the FTOP assumption with NL-GK simulations showed that without flow shear the transport fluxes from the hKBM turbulence are orders of magnitudes above the available heating power and that $(\beta_e, \beta_e')$ is above $(\beta_e, \beta_e')_{\text{crit}}$. Flow shear of the order of $\gamma_E \sim 0.05 - 0.1\ c_s/a$ ($a$: minor radius, $c_s$ sound speed) could bring the heat fluxes down to reasonable levels. The amount of plasma rotation in STEP is very uncertain as the intrinsic rotation in this turbulence regime is not known and the torque input e.g. due to lost $\alpha$-particles is very small. The latter leads to toroidal thermal Mach numbers $|M_{\phi,\text{th}}| = |v_\phi/c_s| < 0.04$, though larger losses due to 3D fields could change this value significantly. A caveat of these local simulations is that they require a rather large radial box size, which may invalidate the local assumption. The first EM global NL-GK simulations with fixed gradients have been performed to verify the applicability of the local simulation and indeed find heat fluxes comparable to those returned by local calculations in the absence of flow shear. Considerable advances have been made in understanding the onset of this transport bifurcation to the high heat fluxes [11]. The low heat flux and electrostatic turbulence states are controlled by zonal flows driven by Reynolds stress restricting the radial extent of the turbulent eddies. As $\beta$ increases the zonal flow damping Maxwell stress becomes more important. This leads to the high transport fluxes observed in the STEP simulations. The onset of this transport state can be characterised by $q^2\beta_{\text{crit}} < C_{\text{nl}}$ where $C_{\text{nl}}$ is a quantity that can be estimated from low $\beta$ electrostatic NL-GK simulations. In addition, the ideal ballooning mode eigenvalue and shear Alfvén wave physics can give a good proxy for the heat flux. This could allow the development of a fast transport model for scenario optimisation.

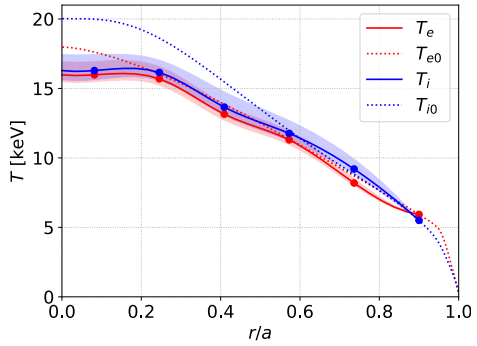


*Figure 2: Predicted temperature profiles for SPP-1 (solid) from hKBM transport using a fixed equilibrium. The dashed line are the initial profiles from the integrated scenario simulation. The bands mark the range of solutions with different assumptions of plasma flow.*

To understand the impact of these findings for the plasma solution, flux driven calculations and full scenario calculations are needed. A new quasilinear reduced model for the hKBM transport (KBM-QL) has been developed and implemented in the transport solver T3D [12]. This transport solver has, for the first time, proven the potential existence of the FTOP solution. The implementation in T3D lacks self-consistency in important areas such as the evolution of the equilibrium and flow as well as the inclusion of $\alpha$-particles and impurities. The calculation starts from the assumed profiles and reaches a high performance FTOP consistent with hKBM turbulent transport, suffering only a small decrease in fusion power by 10% [12]. To achieve this a specific trajectory of flow shear and $\beta_e'$ evolution is needed. In Figure 2 a final comparison between (solid) and (dashed) initial temperature profiles is shown. This transport solution is surprisingly insensitive to plasma rotation (shaded region) but relies heavily on the stabilisation due to $\beta_e'$ especially at the boundary. Whilst this shows the potential existence of a high-performance transport state, the solution is very sensitive to the simulation setup even when approached from a high $(\beta_e, \beta_e')$ state. A full integration into the JINTRAC framework or similar is needed to find a robust path to a viable FTOP and demonstrate access from the low $(\beta_e, \beta_e')$ state. In addition, NL-GK simulations with impurities and $\alpha$-particles have shown that these enlarge the transport fluxes leading to an overall increased heat flux.

## 4. PEDESTAL PHYSICS

For the overall transport state the pedestal pressure is important, which is assumed to be ~15% below the stability limit for type-I edge localised modes (ELMs). This accounts for performance losses due to operating in a no- or small-ELM regime or suppressing ELMs by 3D resonant magnetic field perturbations. The latter has recently been demonstrated on MAST-U $n = 3$ RMP for the first time in an ST [13] albeit in single null (SN). This increases the confidence that RMP ELM suppression could be used in STEP if no/small ELM scenarios cannot be found.

Modelling for SPP-1 and SPP-2 with MARS-Q/F shows that in STEP suppression would be achievable with the dedicated in-vessel coil set behind the blankets with $n = 1,2,3,4$ perturbations using $I_{\mathrm{RMP}} = 10 - 10$ kAt for $n = 1{,}2$ and $I_{\mathrm{RMP}} = 100 - 200$ kAt for $n = 3{,}4$ [14]. This is based on a standard necessary criterion for RMP ELM suppression in SN conventional aspect ratio tokamaks. A strong density pump out has been observed in all of the 5 cases studied (4 SPP-1 and 1 SPP-2). The flow damping for SPP-1 FTOPs ($n = 2$ only) was found to be very strong, whilst the one SPP-2 case has only weak or negligible flow damping.

Access to the edge harmonic oscillation (EHO) was found to be very case sensitive in these 5 cases. The EHO is an indicator if a quiescent H-mode (QH) can be accessed. With the current uncertainties in the edge profiles it is not possible to conclude whether QH-mode could be a viable regime.

Another attractive regime with tolerable edge conditions is the quasi-continuous exhaust mode (QCE). A common hypothesis is that ideal ballooning stability at the separatrix is a good indicator for access to QCE [15,16]. Comparing the STEP edge conditions for SPP-2 to the potential operating space for QCE according [17] (see Figure 3) access to QCE should be possible, though the impact of strong seeding on QCE access is quite uncertain. This is consistent with the STEP edge being in the region of $(\beta_{\mathrm{pol}}, n_{\mathrm{e,sep}}/n_{\mathrm{e,ped}})$ space where QCE is observed on DIII-D. In SPP-1 due to the smaller $R_{\mathrm{geo}}$ and $a$ the projected separatrix operating space was close to the QCE but still in an ELMy region. Evaluating the scaling laws derived for ASDEX Upgrade for the critical normalised pressure gradient $\alpha = \frac{2\delta V}{(2\pi)^2}\left(\frac{V}{2\pi^2 R_{\mathrm{geo}}}\right)^{1/2} \mu_0 p'$ in [16] for STEP we get at the separatrix $\alpha^{\mathrm{sep}}_{\mathrm{edge,crit}} = 0.64\kappa^{2.2}(1+\delta)^{0.9} \approx 10 \ll \alpha^{\mathrm{sep}}_{\mathrm{max,crit}} = 0.57\kappa^{3.3}(1+\delta)^{1.3} \approx 38$ and also at the 95% flux surface $\alpha^{0.95}_{\mathrm{edge,crit}} \approx 9 \ll \alpha^{0.95}_{\mathrm{max,crit}} \approx 29$. This suggest that QCE access should be easy in STEP. The applicability of this scaling for the ST and at high radiation remains uncertain. EUROped was used to compare the infinite n stability boundary with the critical normalised pressure for the peeling ballooning stability. These calculations show that at the separatrix both values are very close to each other. Overall, the evidence is increasing that STEP may be able to operate in QCE during the flat-top. Experimentally access to type-II ELMs (QCE) had already been shown at MAST [18,19] but only transiently in between type-I ELMs. More Stable QCE operation has now been shown in MAST-U [13] opening the possibility to quantify the access criteria in an ST.

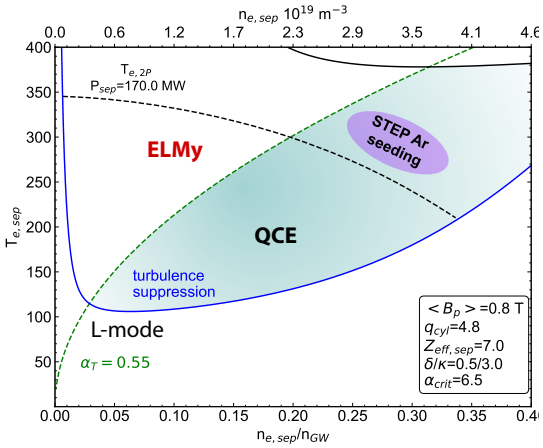


*Figure 3 STEP separatrix conditions for SPP-2 with respect to the separatrix operational space.*

## 5. EXHAUST PHYSICS

SOLPS-ITER simulations without drifts but with kinetic neutrals show that tolerable stationary divertor heat and particle loads require high divertor pressures of $p_{\mathrm{div}} \approx 10 - 20$ Pa and substantial Ar seeding [20], even with divertor geometries having enhanced exhaust capabilities. Ar concentrations at the separatrix of about $c^{\mathrm{sep}}_{\mathrm{Ar}} \approx 3\%$ are needed to reduce the ion temperature to $T_{i,\mathrm{div}} \lesssim 5$ eV to prevent excessive erosion. For SPP-1 the divertor performance was also assessed with SOLPS-ITER simulations including drifts and kinetic neutrals [21]. The effects of the drifts are mostly moderate suggesting easier access to detachment at the inner divertor legs but harder access at the outer legs. Surprisingly the highest heat and particle loads were found in the lower outer divertor despite the ion $\nabla B$-drift being upwards.

The core boundary conditions with respect to the Ar and He concentrations at the separatrix are important for the achievable fusion power. First coupled core edge (COCONUT: JETTO+EDGE2D) calculations for SPP-1 have been started both for He exhaust and Ar concentration separately to assess the impact of the exhaust solution on the core. Both the Ar concentration at the edge as well as the He exhaust are challenging in the SPP-1 divertor geometry. However, the simulations have not yet fully converged giving so far only trends.

Here the separatrix He concentration, $c_{\mathrm{He}}$, is a more difficult problem as the exhaust and the source determined by the fusion performance are strongly coupled and the only control mechanism are the divertor geometry and pumping speed. In contrast for Ar the seeding rates and positions can be optimised for each divertor leg, and a reduction of Ar seeding requirements can be achieved by increasing the divertor pressure with DT puffing. Stand-alone JETTO calculations suggest that to achieve sufficient fusion power, $c^{\mathrm{sep}}_{\mathrm{He}} < 6\%$ at the separatrix is needed whilst for SPP-1 the SOLPS-ITER simulations showed $c^{\mathrm{sep}}_{\mathrm{He}} \sim 12\%$ [22] confirmed by the coupled calculations with pumping speeds $S_{\mathrm{He}} \geq 50\ \mathrm{m}^3/s$ [23]. To stabilise the coupled calculations $\beta_N$ was controlled leading to a change in the confinement assumption the impact of which was explored with JETTO only calculations varying

the core confinement and pedestal assumptions. The combined study shows that pumping speeds of $S_{\mathrm{He}} = (53 \pm 20)\mathrm{m}^3/\mathrm{s}$ would be sufficient in the SPP-1 design to achieve adequate He exhaust to reach $c_{\mathrm{He}}^{\mathrm{sep}} < 6\%$.

Routes for improvements of the He exhaust in SPP-1 have also been studied with SOLPS-ITER [22] by varying the pump duct location with a fixed pumping speed of $S_{\mathrm{He}} = 24\ \mathrm{m}^3/\mathrm{s}$. On STEP pumping is only possible from the outer divertor chambers. The baseline design has a pumping duct in the outer SOL and the strike-point on a horizontal target. The $c_{\mathrm{He}}^{\mathrm{sep}}$ is dominated by the inner divertor leg and He is entering the core through the X-point region. Moving the duct location into the private flux region and changing the outer divertor geometry to a vertical target reduces the He concentration by about a factor of two. Only with a pump duct close to the strike point in the corner is the He concentration reduced to sufficiently low levels. In such a pumping configuration very high DT puffing would be needed in the divertor likely inconsistent with safety limits imposed by the fuel cycle. These calculations neglected important physics as has been shown in [24]. Repeating them with the model by Zhdanov et. al. [25] leads to a significant reduction of $c_{\mathrm{He}}^{\mathrm{sep}}$ as already observed for ITER simulations. The latest simulations for SPP-2 suggest that $c_{\mathrm{He}}^{\mathrm{sep}}$~4% can be achieved with $S_{\mathrm{He}} = 24\ \mathrm{m}^3/s$.

## 6. CURRENT DRIVE PHYSICS

The NI scenarios are very sensitive to the current drive efficiency and minimising the microwave power needed for current drive at high density is key to the success of STEP. On the plasma side electron Bernstein wave current drive (EBCD) offers the possibility to increase the normalised off-axis current drive efficiency by a factor 2 – 3 with respect to ECCD. The physics of EBCD is much more complicated and at much lower maturity level than for ECCD. For EBCD scenario simulations the development of ray tracing tools is needed to optimise launch geometries and frequencies. The tools matured for ECCD such as GRAY, TORBEAM and GENRAY lack important physics and often full Fokker-Planck modelling (e.g. with CQL3D [26]) is needed to calculate the current drive efficiency. CRAYON, is a new fast relativistic ray tracing tool, developed to close the gaps in EBCD ray-tracing [27]. Several important issues are tackled allowing for a rapid evaluation of the current drive in the linear limit (100 – 1000 times faster than CQL3D). As electron Bernstein waves couple efficiently to the fast electrons in the tail of the velocity distribution relativistic effects become important under reactor like conditions [28]. Indeed, STEP calculations show that with relativistic effect included EBCD rays are predicted to reach much deeper into the plasma than without [28]. The common ray-tracing tools used for ECCD are usually limited to one mode but EBCD relies on O-X-B mode conversion from the launched electromagnetic O-mode wave at the cut-off layer to X-mode and finally at the upper hybrid resonance. The simple schemes used for example in GENRAY can cause "premature ray teleportation" that can lead to large errors on the deposition as ray tracing errors accumulate. A more robust asymptotic matching technique will be used in CRAYON as well as analytic derivates of the hot plasma kinetic dispersion relation for higher accuracy of the ray propagation. The analytic approach will also lead to an improved speed of the code. Finally, for EBCD the rays are slowed down at the conversion layer, and the electric fields are strongly enhanced. Therefore, the collisional damping plays a crucial role in colder plasmas such as MAST-U or TCV, which will be used to validate the simulations for STEP.

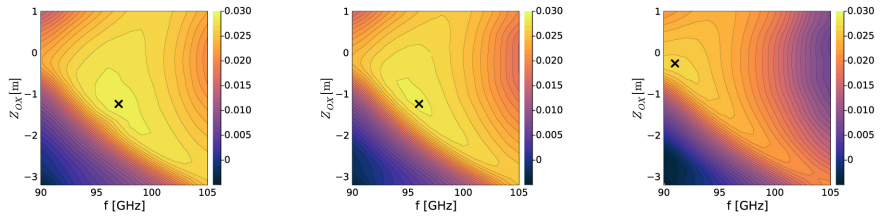


(a) $P_{\mathrm{EBW}}$ =1MW (b) $P_{\mathrm{EBW}}$ =10MW (c) $P_{\mathrm{EBW}}$ =100MW

*Figure 4: Global current drive efficiency $\eta_{EB} = I_{CD}/P_{EBW}$ $(A/W)$ as function of frequency and launch height for different microwave powers (a – c). The black cross marks the $(f, Z_{OX})$ for the highest $\eta_{CD}$.*

Another important effect for ECCD caused by coupling to the tail of the distribution is the non-linearity arising from the modification of the velocity distribution by the absorption itself. Under STEP conditions comparison of the linear modelling with CQL3D has shown that for ECCD this already has an impact at powers $P_{\mathrm{EBW}} \gtrsim 1$ MW [28]. Only the damping is affected but not the ray trajectory. Figure 4 shows absolute EBCD efficiencies $\eta_{\mathrm{EB}}$ for different $P_{\mathrm{EBW}}$ from CQL3D for SPP-1 as function of frequency, $f$, and launch height, $Z_{\mathrm{OX}}$ around the values derived from the linear approximation. For $P_{\mathrm{EBW}} > 10$ MW the current drive efficiency is reduced in this case, and the launch point is shifted to lower $f$ and higher $Z_{\mathrm{OX}}$ . Also, the radial deposition location moves inward showing the importance of relativistic effects. A key caveat of these calculations is that the electron transport is not calculated self-consistently but is described by a diffusion coefficient that usually needs to be derived in comparison with experiments.

The optimisation of the current drive efficiency $\eta_{\mathrm{CD}}$ over the plasma radius is a complex integrated problem. E.g. for SPP-2 optimising the pellet trajectory as well as the pedestal performance has led to an increase in the $\eta_{\mathrm{CD}}$ for

the EBCD scenario recovering the EB-HQ scenario (see section 2). However, without predictive modelling there remains an uncertainty in the actual current drive performance and the validity of the optimum launch geometry.

## 7. MHD CONTROL AND DISRUPTIONS

STEP relies on high $\beta_N$ and $\kappa$ to achieve sufficient $P_{\text{fus}}$ in a relative compact design. The current FTOPs require both resistive wall mode and vertical control (as any shaped tokamak). In general, to achieve the same $P_{\text{fus}}$ in SPP-2 a lower $\beta_N$ than in SPP-1 is required. The lower pedestal performance, however, requires a higher pressure peaking. Together with the changed current drive profiles due to the changed profile shapes this leads to a higher $C_\beta = (\beta_N - \beta_N^{\text{nw}})/(\beta_N^{\text{iw}} - \beta_N^{\text{nw}})$ ($\beta_N^{\text{nw}}, \beta_N^{\text{iw}}$: no-wall and ideal wall limit respectively) in SPP-2 than in SPP-1. $C_\beta < 0.5$ is a design metric for the RWM controllability. For SPP-1 $n = 1{,}2$ successful RWM control in the presence of reasonable sensor noise has been simulated with MARS-F for a scenario with $C_\beta = 0.6$ and $\beta_N = 5.1$. The current FTOPs shown in Figure 1 need further profile optimisation to meet this target except surprisingly for the low radiation fraction scenario. Again, the pedestal performance becomes an important optimisation factor.

The operation in DN has the key function to shield the inner divertor from excessive heat loads. For this the upper and lower X-point need to be ideally on the same flux surface. A key challenge for the vertical control in DN is to keep the separation of the two flux surfaces for the upper $\psi_X^u$ and lower $\psi_X^l$ X-point, $\Delta\psi_{\text{ul}} = \psi_X^u - \psi_X^l$ as small as possible during the unavoidable control related vertical oscillations. Usually, $\Delta\psi_{\text{ul}}$ is translated to the flux separation in R at the outer midplane $\Delta R_{\text{sep}}$. Failing to keep $|\Delta R_{\text{sep}}| < \lambda_q \sim 1 - 2$ mm ($\lambda_q$: SOL power decay length) will lead to transient heat load variations in the four divertor legs that could lead to re-attachment. In addition, if the plasma moves into a SN configuration with the ion $\nabla B$-drift away from the X-point on the last closed flux surface H-mode could be lost [29,30]. The absolute accuracy required for the vertical control becomes more challenging with increasing device size as the underlying length scales don't scale favourably with device size. A novel vertical control scheme has been developed that allows simultaneous control of the vertical position as well as $\Delta\psi_{\text{ul}}$ [31]. Initial, tests of this scheme have been done on TCV showing that even with a very simple control algorithm good control of $\Delta\psi_{\text{ul}}$ can be achieved during vertical shifts of the plasma of up to $\Delta Z \leq 3$ cm.

Disruptions and the associated generation of a runaway electron (RE) beam due to the avalanche mechanism are one of the biggest threats to tokamak based fusion power plants as well as ITER. At the plasma currents needed to reach sufficient $Q_{\text{fus}}$ it is nearly impossible to avoid RE currents of the order of several MA without mitigation. Controlling the current and thermal quench in STEP with shattered pellet injection (SPI) seems feasible [32]. Using SPI to mitigate the RE beam may not be possible, though STEP seems close to the benign regime. Re-initiation by seed electrons from Compton scattering or T decay is also a key concern, similar to ITER. Therefore, initial studies of the requirements for a single turn $n = 1$ RE mitigation coil (REMC) [33] for SPP-2 have been done. The deconfinement of the RE in mock equilibria with $E_{\text{el}} = 0.1 - 10$ MeV electron markers was simulated with the LOCUST [34] code [35]. Two extreme equilibria have been studied. A full bore flattop like equilibrium with $I_p = 21$ MA and a smaller circular RE like equilibrium with $I_p = 12$ MA. To deconfine 100% of the marker electrons $1.2\text{ MA} \leq I_{\text{REMC}} \leq 1.6\text{ MA}$ are needed for the given coil configuration, which leads to considerable forces on the coil. The impact on the engineering design of such a structure is currently being assessed.

## 8. PLASMA INITIATION, RAMP-UP AND DOWN

Both SPP-1 and SPP-2 have a small solenoid to aid plasma initiation and the generation of a suitable diverted target for the NI ramp-up. Plasma break-down and burn-through is modelled with the DYON code in close collaboration with the coil and power supply engineers to ensure a conformant design. Optimised field configurations with a high-level field null including an assessment of the eddy currents in the major conducting structures are provided by an optimisation algorithm implemented to the FIESTA code. The DYON code has now been validated against several different devices including MAST-U [36]. The SPP-2 modelling shows that without the assistance of ECRH $V_{\text{loop}} \geq 15$ V and a solenoid flux of about $\Delta\psi_{\text{CS}}^{\text{ini}} \sim 5$ Vs is needed for a successful initiation at $p_{\text{pre}} = 1$ mPa and 1% Oxygen. This is about twice as much as needed in SPP-1. A key aspect for the higher requirements is the large vacuum vessel volume. JETTO modelling with simplified assumptions shows that for the following inductive phase depending on the ramp speed a further $\Delta\psi_{\text{CS}}^{\text{lim}} \approx 10 - 15$ Vs is needed.

The strategies for the NI ramp-up and ramp-down have not been changed with respect to SPP-1. For the ECCD ramp-up the full current will be generated using the lowest possible density compatible with detached divertor operation. A densification phase at full current is envisaged to access the fusion conditions. Initial predictive modelling for this phase in SPP-1 has been performed. The low-density phase is modelled with a TGLF surrogate model especially developed for STEP (TGLFNN) using the TGLF optimised for ST conditions [37]. TGLFNN compares well to full TGLF modelling throughout the ramp (see Figure 5). Also, first predictive simulations for the densification phase have been attempted showing that this highly non-linear phase requires fine simulation feedback control. Pathways from the control point of view through this phase have been explored using the RAPTOR code with the simplified BgB model. The onset of the plasma burn is also a critical phase for the wider

plant. From the plasma point of view the onset should be as fast as possible as the competition between the increase in bootstrap current and the decrease in ECCD current drive efficiency makes maintaining the plasma current difficult. The initial strategy to ramp the density up in about 10s would have led to a very complicated thermal management system in the wider plant and a slower densification phase is now pursued.

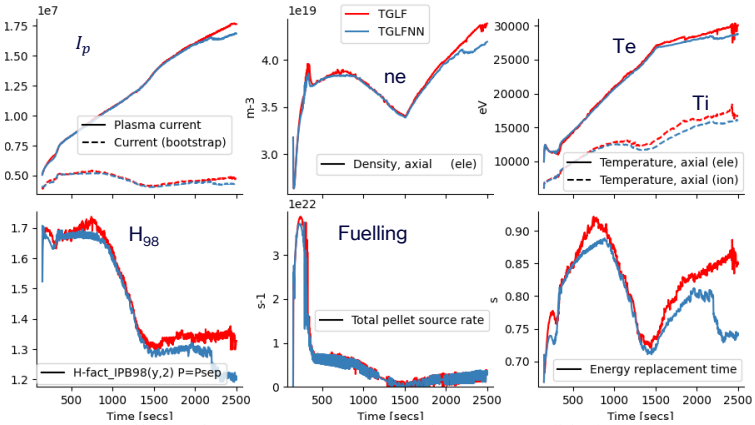


*Figure 5: Fully predictive NI ramp-up simulation using (blue) TGLFNN.v1 in comparison with (red) full TGLF as transport model in JETTO as proof of principle.*

In both the ramp-up and ramp-down phases maintaining vertical stability and acceptable divertor conditions will be key constraints. Better control capabilities for the JETTO modelling are being implemented to make the search for robust ramp-up and ramp-down trajectories more efficient. Fast models to assess divertor conditions and vertical stability have also been developed and are used in post-processing.

## 9. BURN CONTROL

A potential fusion power plant must be able to control the power output to the grid. This defines plasma burn control – varying $P_{\mathrm{fus}}$ – as one of the key functions for the plasma system. During the variation of the fusion output a safe plasma state must be maintained. The strong non-linear coupling of the plasma especially for a fully non-inductive operating state is a significant control challenge and needs to be integrated into the plasma and machine design from the start. Novel trajectory optimisation and control methods have been developed to address this challenge [38]. Using the RAPTOR code for the first time simultaneous control of the $\alpha$-power $P_\alpha = P_{\mathrm{fus}}/5$, the q-profile and the internal inductance $l_i(3)$ has been demonstrated on a fully NI plasma state. For this also a Dirichlet boundary condition for the poloidal flux diffusion equation was introduced in RAPTOR allowing the plasma boundary flux rather than the plasma current to be used as an actuator as well as other significant improvements to the code. A novel multi-objective approach was used to understand the optimal control. The ECCD power and pellet fuelling (modelled as continuous fuelling) were used as the main actuators with constraints such as $q_{\mathrm{min}} > 2$ and $f_{\mathrm{GW}} < 1$ and a maximum $l_i(3) < 0.4$ to maintain a stable plasma state. An unrealistically fast temporary ($\Delta t = 300$ s) step down of $\Delta P_\alpha = 240$ MW from $P_\alpha = 340$ MW was modelled to test the optimised system response. There is a clear trade-off between the q, $l_i(3)$ and $P_\alpha$ tracking errors. Good simultaneous tracking of both $l_i(3)$ and $P_\alpha$ cannot be achieved within the 300 s optimisation horizon with any set of objective function weighting values. The fast step down in $P_\alpha$ can be reasonably realised, but the step up takes about 250 s due to the constraint violations in the step down. Confidence has been gained in the performance of the optimised objective function which will be used in a future closed loop model-predictive control framework.

## 10. LOWER ELONGATION ALTERNATIVES

As discussed in section 7 the operation at $\kappa \approx 3$ poses significant challenges on the design of the scenario and the vertical control system. Using the scenario assumption workflow without q-profile optimisation the impact of operating at lower elongation have been studied. Based on the SPP-2 EC-HD scenario the elongation has been varied between $1.85 \leq \kappa \leq 3.3$ at fixed $P_{\mathrm{fus}}$~1.7 GW, plasma volume $V_{\mathrm{pl}}$, $f_{\mathrm{GW}}$~1, $B_t(R_{\mathrm{geo}}) = 3$ T and $A = 1.8$. This leads to a larger major radius at lower elongation. A second scan maintaining $R_{\mathrm{geo}}$ but reducing the plasma volume has also been done. The $\kappa = 2.5$ points for each scan have gone through the full FTOP optimisation to define suitable reference points. Both scans show that as the elongation decreases, higher values of $\beta_N$, and stronger confinement – exemplified by the H factor –are required to maintain the fusion power. Although the bootstrap current fraction drops with lower elongation this is partially offset in the constant-volume scan by improved ECCD efficiency resulting from the reduced plasma density. There is also a slight decrease of $I_p$ with decreasing elongation. The scan at fixed $R_{\mathrm{geo}}$ leads to a stronger increase of $\beta_N$ as the volume decreases. The optimisation of the q-profile with $q_{\mathrm{min}} \geq 2.3$ led to even higher $\beta_N$, though this does not necessarily mean that $C_\beta$ becomes worse.

From a simplistic geometric view, one might expect a reduction in Tritium breeding ratio, but simple neutronics assessments of the lower elongation scenarios have shown only a negligible impact. Nevertheless, the higher

confinement assumption, larger $R_{geo}$ and/or likely more challenging RWM stability with marginal improvement of the vertical stability challenge led to the decision not to pivot to a lower elongation design.

## 11. CONCLUSIONS

In conclusion, the plasma scenario and control work continue to reduce the uncertainty of the plasma solution for STEP. Tools and workflows have been developed to re-evaluate efficiently any design changes, and these are progressively being further optimised to increase modelling fidelity. For example, core transport solutions can now be based on predictive modelling though important features are still missing, such as fusion $\alpha$-particles and impurities. Furthermore, the plasma design is strongly integrated with the engineering effort – a key aspect of successful power plant design.

## ACKNOWLEDGEMENTS

This work has been funded by STEP, a UKAEA programme to design and build a prototype fusion energy plant and a path to commercial fusion. To obtain further information on the data and models underlying this paper please contact PublicationsManager@ukaea.uk.

## REFERENCES

[1] C. Waldon, S. I. Muldrew, J. Keep, R. Verhoeven, T. Thompson, and M. Kisbey-Ascott, Philosophical Transactions of the Royal Society A: Mathematical, Physical and Engineering Sciences **382**, 20230414 (2024).
[2] H. Meyer and o. b. o. t. S. P. Team, Philosophical Transactions of the Royal Society A: Mathematical, Physical and Engineering Sciences **382**, 20230406 (2024).
[3] M. Lennholm *et al.*, Philosophical Transactions of the Royal Society A: Mathematical, Physical and Engineering Sciences **382**, 20230403 (2024).
[4] S. Freethy, L. Figini, S. Craig, M. Henderson, R. Sharma, T. Wilson, and S. t. the, Nuclear Fusion **64**, 126035 (2024).
[5] E. Tholerus *et al.*, Nuclear Fusion **64**, 106030 (2024).
[6] J. Acres and C. Clements, in *Turbo Expo* (ASME, London, United Kingdom, 2024).
[7] P. T. Lang *et al.*, Nuclear Fusion **52**, 023017 (2012).
[8] S. Ding *et al.*, Nature **629**, 555 (2024).
[9] H. Meyer, in *Magnetic Fusion Energy: From Experiments to Power Plants*, edited by G. H. Neilson (Woodhead Publishing (Elsevier), 2016), pp. 359.
[10] M. Giacomin, D. Kennedy, F. J. Casson, A. C J, D. Dickinson, B. S. Patel, and C. M. Roach, Plasma Physics and Controlled Fusion **66**, 055010 (2024).
[11] D. Kennedy, in *30th IAEA Fusion Energy Conference*Chengdu, China, 2025).
[12] M. Giacomin *et al.*, Journal of Plasma Physics **91**, E16, E16 (2025).
[13] J. Harrison, in *30th IAEA Fusion Energy Conference*Chengdu, China, 2025).
[14] Y. Liu, X. Chen, Z. Li, S. Saarelma, T. Tang, and G. Xia, Plasma Physics and Controlled Fusion **67**, 085010 (2025).
[15] G. F. Harrer *et al.*, Nuclear Fusion **58**, 112001 (2018).
[16] M. Dunne, M. Faitsch, L. Radovanovic, E. Wolfrum, and A. U. T. the, Nuclear Fusion **64**, 124003 (2024).
[17] T. Eich *et al.*, Nuclear Materials and Energy **42**, 101896 (2025).
[18] R. Maingi, A. E. Hubbard, H. Meyer, J. W. Hughes, A. Kirk, R. Maqueda, J. L. Terry, M. the Alcator C-Mod, and N. teams, Nuclear Fusion **51**, 63036 (2011).
[19] A. Kirk *et al.*, Plasma Physics and Controlled Fusion **53**, 95008 (2011).
[20] S. S. Henderson *et al.*, Nuclear Fusion **65**, 016033 (2025).
[21] J. Karhunen, S. S. Henderson, A. Järvinen, D. Moulton, S. Newton, and R. T. Osawa, Nuclear Fusion **64**, 096021 (2024).
[22] R. Osawa, in *51st EPS Conference on Plasma Physics*Vilnius, Lithuania, 2025).
[23] E. Tholerus, in *30th IAEA Fusion Energy Conference*Chengdu, China, 2025).
[24] A. Zito *et al.*, Nuclear Fusion **65**, 046022 (2025).
[25] S. O. Makarov *et al.*, Nuclear Fusion **63**, 026014 (2023).
[26] R. W. Harvey and M. G. McCoy, pp. 489.
[27] T. Wilson, in *51st EBS Conference on Plasma Physics*Vilnius, Lithuania, 2025).
[28] B. Biswas, S. Freethy, and R. Vann, Nuclear Fusion **65**, 016010 (2025).
[29] H. Meyer *et al.*, Nuclear Fusion **46**, 64 (2006).
[30] H. Meyer *et al.*, Plasma Physics and Controlled Fusion **50**, 15005 (2007).
[31] M. Lafferty, in *IEEE Symposium on Fusion Engineering (SOFE)*Boston, USA, 2025).
[32] A. Fil, L. Henden, S. Newton, M. Hoppe, and O. Vallhagen, Nuclear Fusion **64**, 106049 (2024).
[33] A. H. Boozer, Plasma Physics and Controlled Fusion **53**, 084002 (2011).
[34] S. H. Ward, R. Akers, A. S. Jacobsen, P. Ollus, S. D. Pinches, E. Tholerus, R. G. L. Vann, and M. A. Van Zeeland, Nuclear Fusion **61**, 086029 (2021).
[35] J. Morris, in *Runaway Mitigation Meeting*EPFL, Lausanne, Switzerland, 2025).
[36] H.-T. Kim, in *30th IAEA Fusion Energy Conference*Chengdu, China, 2025).
[37] F. Casson, in *29th EU-US TTF Transport Task Force Workshop*Budapest, Hungary, 2025).
[38] J. Mitchell *et al.*, Fusion Engineering and Design **219**, 115202 (2025).